AIP | The Journal of Chemical Physics

Electron hole pair mediated vibrational excitation in CO scattering from Au(111): Incidence energy and surface temperature dependence

Pranav R. Shirhatti, Jörn Werdecker, Kai Golibrzuch, Alec M. Wodtke, and Christof Bartels

Citation: The Journal of Chemical Physics **141**, 124704 (2014); doi: 10.1063/1.4894814
View online: http://dx.doi.org/10.1063/1.4894814
View Table of Contents: http://scitation.aip.org/content/aip/journal/jcp/141/12?ver=pdfcov
Published by the AIP Publishing

Electron hole pair mediated vibrational excitation in CO scattering from Au(111): Incidence energy and surface temperature dependence

Pranav R. Shirhatti,[1,2] Jörn Werdecker,[1,2,a)] Kai Golibrzuch,[1,2] Alec M. Wodtke,[1,2] and Christof Bartels[1,2,b)]

[1]*Institute for Physical Chemistry, Georg August University of Göttingen, 37077 Göttingen, Germany*
[2]*Max Planck Institute for Biophysical Chemistry, 37077 Göttingen, Germany*

(Received 27 June 2014; accepted 19 August 2014; published online 24 September 2014)

We investigated the translational incidence energy (E_i) and surface temperature (T_s) dependence of CO vibrational excitation upon scattering from a clean Au(111) surface. We report absolute $v=0\rightarrow 1$ excitation probabilities for E_i between 0.16 and 0.84 eV and T_s between 473 and 973 K. This is now only the second collision system where such comprehensive measurements are available – the first is NO on Au(111). For CO on Au(111), vibrational excitation occurs via direct inelastic scattering through electron hole pair mediated energy transfer – it is enhanced by incidence translation and the electronically non-adiabatic coupling is about 5 times weaker than in NO scattering from Au(111). Vibrational excitation via the trapping desorption channel dominates at $E_i = 0.16$ eV and quickly disappears at higher E_i. © *2014 AIP Publishing LLC*. [http://dx.doi.org/10.1063/1.4894814]

INTRODUCTION

Studying vibrational energy transfer between small molecules and well defined surfaces provides insights into mechanisms of energy flow relevant to adsorbate surface chemistry.[1–3] For example, Kay and co-workers[4] have shown that the vibrational excitation probability of NH_3 (umbrella mode) scattered from a Au(111) surface increases monotonically with the translational incidence energy (E_i) above a threshold close to the vibrational excitation energy. The surface temperature (T_s) had no influence on the vibrational excitation probability. Here, vibrational excitation occurs via direct coupling to the translational incidence energy in an electronically adiabatic manner. On the other hand, NO scattering from Ag(111)[5] and Au(111)[6,7] surfaces showed vibrational excitation that is strongly enhanced by surface temperature, following a pseudo-Arrhenius law where the effective activation energy is the vibrational excitation energy. While the translational incidence energy of NO molecules also enhanced vibrational excitation, no threshold was observed. In this case, the vibrational excitation occurs via coupling of the molecular vibration to the hot electron hole pairs of the metal (EHP-V).

The EHP-V energy transfer observed for NO/Ag(111) and NO/Au(111) is an example of the breakdown of the Born-Oppenheimer approximation (BOA).[8] The availability of detailed experimental data especially for NO/Au(111),[6,9,10] has triggered the development of several theoretical approaches that go beyond the BOA, explicitly describing the coupling of nuclear and electronic degrees of freedom.[2,11–14] Extending the study of EHP-V energy transfer to other systems addresses questions of generality and validity for post-Born-Oppenheimer theories.

In this paper, we report comprehensive measurements of absolute vibrational excitation probabilities for the recently reported EHP-V energy transfer for CO collisions with Au(111).[15] This system behaves similarly to NO on Ag/Au, but it is complicated by the presence of trapping/desorption, which is important at low E_i.[16] Making use of absolute vibrational excitation probabilities, we characterize the two channels contributing to vibrational excitation of CO on Au(111).

METHODS

Some essential features of the experimental set-up are provided in the following paragraphs. For a more detailed description the reader is referred to Ref. 17. A schematic diagram of the experimental set-up is shown in Fig. 1.

The apparatus consists of four interconnected chambers: (1) source chamber, (2) differential pumping-1 stage, (3) differential pumping-2 stage, and (4) UHV surface science chamber. In the source chamber, a supersonic jet expansion of the CO molecules with a suitable carrier gas (H_2/Ne) was produced using a home-built, piezo-electrically driven pulsed nozzle (stagnation pressure: 3 bars, temperature: 300 K, nozzle diameter: 1 mm). The expanding gas passes through a skimmer (1.5 mm opening diameter, Beam Dynamics) and subsequently through two circular apertures of 3 mm and 2 mm diameters, respectively, before it enters the UHV chamber as a collimated molecular beam. The typical duration (FWHM) of the molecular beam is 100–150 μs when it collides with the Au(111) surface, which is placed ~180 mm away from the pulsed valve opening. Typically, the pressure in the UHV chamber was 2×10^{-10} Torr and 2×10^{-9} Torr (unscaled ion gauge readings) with the molecular beam off and on, respectively. The mean E_i of the CO molecules was varied in the range of 0.16–0.84 eV by using different mixing ratios and carrier gases (Table I). The fraction of the molecules in

a)Present address: Laboratoire de Chimie Physique Moléculaire, Ecole Polytechnique Fédérale de Lausanne, 1015 Lausanne, Switzerland.
b)Author to whom correspondence should be addressed. Electronic mail: cbartel@gwdg.de

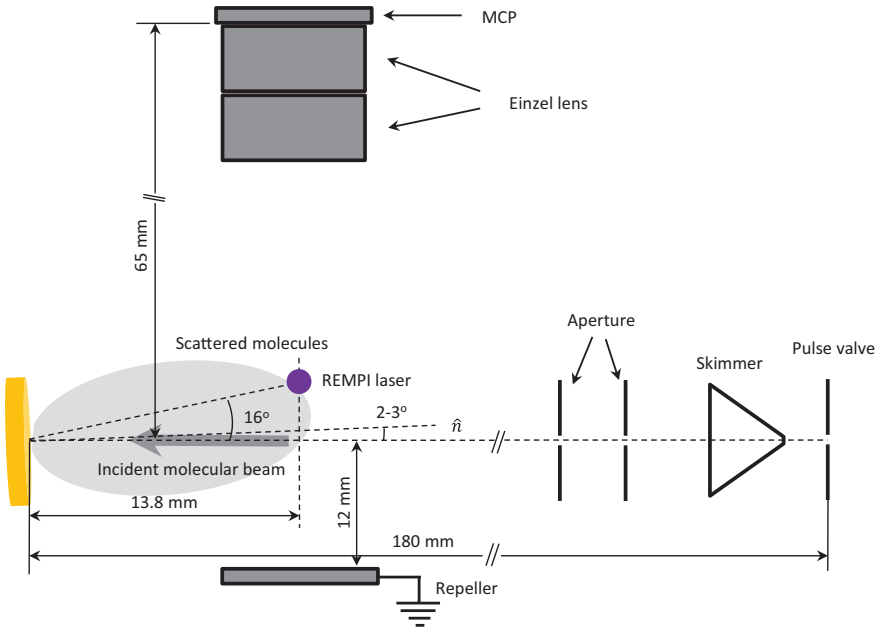

FIG. 1. A schematic diagram of the experimental set-up. A supersonic expansion of the CO molecules with suitable carrier gas is produced by the pulse valve. This expansion is made to pass through a skimmer and two apertures downstream to obtain a collimated molecular beam before it collides with the Au(111) surface. The surface was tilted upwards (2°–3°) in these experiments. The scattered molecules were detected at a position vertically offset from the incident beam (∼10° from the specular angle) in order to minimize the background caused by the non-resonant ionization of the incident beam.

the $v = 1$ state in the incident molecular beam was measured to be less than 10^{-4}.

The Au(111) single crystal (orientation accuracy < 0.1°, purity 99.999%, MaTeck GmbH) is housed in the UHV chamber, mounted on a sample holder with tungsten wires. The crystal can be conductively heated by resistively heating the tungsten wires. The temperature is monitored by a K-type thermocouple attached on the edge of the crystal. Prior to each set of measurements for a given incidence energy, the surface was cleaned by sputtering with 3 keV Argon ions for 20–25 min. Subsequently, the crystal was annealed at 970–1000 K for 30–40 min to recover the (111) surface. The surface cleanliness was checked using Auger electron spectroscopy.

The molecular beam was incident on the surface at 2°–3° away from normal incidence and the scattered molecules were detected at a position vertically offset from the incident beam (∼10° from the specular reflection angle, see Fig. 1). This offset along the vertical axis minimizes background signal arising from the non-resonant ionization of the incident molecular beam. The CO molecules in the $v = 0$ and $v = 1$ states (ground electronic state) were detected using a 2+1 Resonantly Enhanced Multiphoton Ionization (REMPI) scheme via the $B\,^1\Sigma^+$ state. The resulting ions were extracted using a combination of two electrostatic lenses and a grounded repeller plate. These ions were detected using a dual micro channel plate (MCP) detector, with the plates arranged in a Chevron configuration.

TABLE I. Characteristics of the molecular beams used in the experiments. $\langle E\rangle$ denotes the mean value and $\Delta E/\langle E\rangle$ denotes the width of the energy distribution, where $\Delta E = \sqrt{\int (\langle E\rangle - E)^2 dE}$. The typical fraction of the molecules in the $v = 1$ state in the incoming beam was <0.01%.

Gas mixture composition	$\langle E\rangle$ (eV)	$\Delta E/\langle E\rangle$ (%)
2% CO + 98% H_2	0.84	8.6
5% CO + 95% H_2	0.65	8.4
10% CO + 90% H_2	0.50	8.7
15% CO + 85% H_2	0.42	9.4
20% CO + 80% H_2	0.34	8.8
4% CO + 36% H_2 + 60% Ne	0.16	7.0

Calculation of the absolute vibrational excitation probability

The approach used for calculating the absolute vibrational excitation probability is similar to that used earlier for NO scattering from Au(111) and CO scattering from Au(111).[7,15] The key features of this method are outlined briefly below.

The vibrational excitation probability in this work is defined by the following equation,

$$P(v = 0 \rightarrow i) = \frac{N_i}{\Sigma_j N_j},$$

where N_i is the population in the ith vibrational state in the scattered beam. In the present case of CO ($v = 0$) scattering from a Au(111) surface, for the temperature range studied (473–973 K), the molecules largely scatter back in $v = 0$ and a small fraction (<1%) of the molecules scatter back in $v = 1$. The population in the higher vibrational states is negligibly small. Thereby, the above equation can be reduced to the following:

$$P(v = 0 \rightarrow 1) \cong \frac{N_1}{N_0 + N_1}.$$

The practical implementation of this scheme requires the measurement of N_i (or a quantity proportional to it) for

$i = 0$ and 1. It should be noted that the population of the scattered molecules in the $v = 0$ and 1 states are distributed over a large number of rotational states. Additionally, the scattered molecules also arrive with a temporal and angular distribution that, in general, can depend on the final vibrational state. Hence, it is necessary to account for these effects in the evaluation of the vibrational excitation probabilities. The measured signals also have to be scaled to account for differences in experimental parameters such as the laser power and the MCP gain. This enables us to make a meaningful comparison among the different datasets.

The scattering rotational state distributions in $v = 0$ and 1 were obtained by measuring the 2+1 REMPI spectra via the $B\,^1\Sigma^+$ state using the Q(0,0) and Q(1,1) bands, respectively. Since the Q(1,1) branch lines overlap the O(0,0) lines, the observed spectra were fit to a sum of O(0,0) and Q(1,1) lines and the Q(1,1) component was extracted. In these measurements, the REMPI laser was set at a fixed delay with respect to the nozzle opening time. These measurements were carried out at 11 different surface temperatures ranging from 473 to 973 K in steps of 50 K.

The arrival time distributions of the scattered molecules in $v = 0$ and 1 (at different surface temperatures) were measured by scanning the REMPI laser in time with respect to the incoming pulsed beam. The angular distributions of the scattered molecules were measured by moving the REMPI beam along a plane perpendicular to the incident beam, covering scattering angles from approximately -40° to 40° from the surface normal. For detection of $v = 0$, the REMPI wavelength was chosen such that the high J states (populated only in the scattered beam) were detected.

Estimation of uncertainties

The major uncertainty in the measurements arises from fluctuations in the laser power, which were measured to be about 5%. In addition, error is introduced due to variations in MCP gain caused by the variation in the MCP voltage, which was measured to be of the order of ~0.5%. Uncertainties in the fitting parameters were also taken into account. The individual errors were propagated using Gaussian error propagation (assuming that the errors are independent and random) to estimate the uncertainties in the derived vibrational excitation probabilities. The reported error bars are 95% confidence intervals.

RESULTS AND DISCUSSION

Some examples of the REMPI spectra of the scattered CO molecules in the Q(1,1) band region measured at different surface temperatures and translational incidence energies are shown in Fig. 2. Clearly, the intensity of the Q(1,1) band increases with increasing surface temperature.

In order to quantify the change in the CO $v = 1$ population in the scattered flux as a function of T_s, the integrated intensity of the Q(1,1) band has to be evaluated. Since the Q(1,1) band is overlapped with the nearby O(0,0) branch lines, we fitted the observed REMPI spectra to a sum of the Q(1,1) and the O(0,0) spectra using the intensity of each band

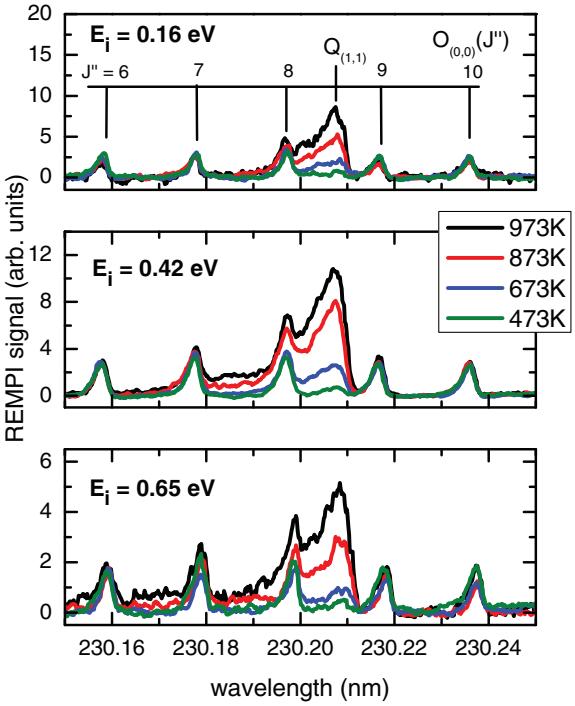

FIG. 2. Examples of REMPI spectra of the scattered CO ($v = 1$) molecules measured via the Q(1,1) band at different surface temperatures for three different E_i. Clearly, for a given E_i it can be seen that the intensity of the Q(1,1) band increases with T_s, whereas the intensity of the nearby O(0,0) branch lines does not.

as a fit parameter. The best fit parameters were used to evaluate the Q(1,1) spectrum and its integrated value. The Q(0,0) band was integrated directly (numerically) as the overlapping S(0,0) band has negligible intensity (relative to the Q(0,0) band).[18]

Both the $v = 0$ and 1 rotational distributions show deviations from a thermal distribution and depend strongly on E_i, consistent with direct inelastic scattering (see Fig. 3).[19] Hence, Q(1,1) and Q(0,0) bands were fit using an empirical non-thermal rotational state distribution of the following form,

$$N(J) = F_{th}(J, T_{rot}) + a_r \times \exp\,[-((J - a_0)/a_1)^2],$$

where F_{th} is a Boltzmann distribution and the second term represents a non-thermal component produced by a rotational rainbow. The non-thermal component is modelled as a Gaussian function with the parameters a_r, a_0, and a_1 representing its amplitude, center, and width, respectively. The quantities a_r, a_0, and a_1 and T_{rot} were obtained from fitting the observed spectra. Few examples of the fit are shown in Fig. 3 (lower panel). Additional fits and the best fit parameters obtained are provided in the supplementary material.[20]

The angular distributions were measured both as a function of E_i and T_s and some of these results are shown in Fig. 4. The CO angular distributions for both $v = 0$ and 1 were narrower than a cosine function – shown as red dashed curve in Fig. 4 – indicating that a majority of the molecules undergo direct inelastic scattering. It can also be seen that the angular distributions for the scattered CO molecules in the $v = 1$ state are broader than those for $v = 0$. Moreover, the angular

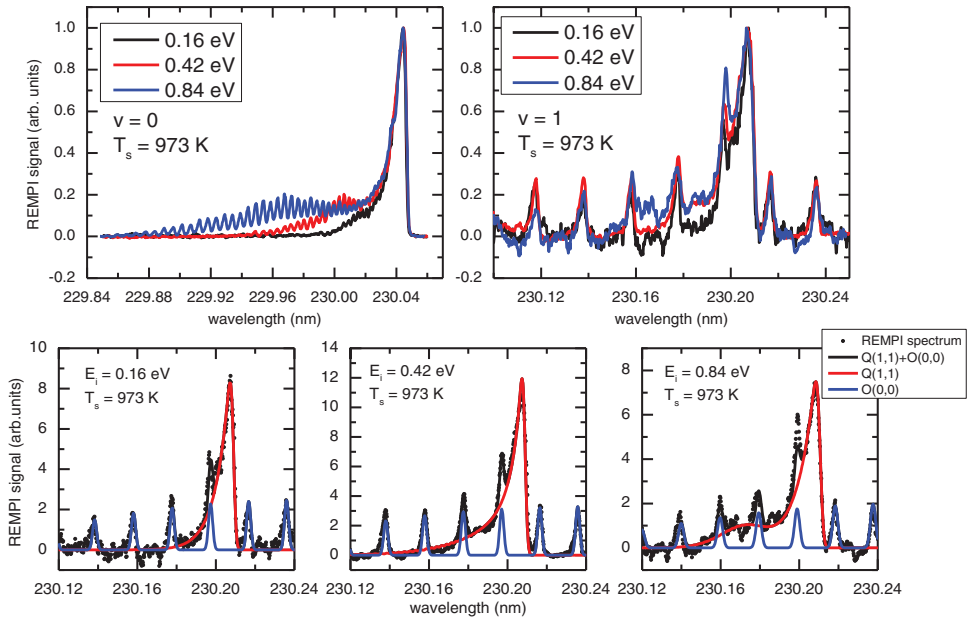

FIG. 3. (Upper panel) REMPI spectra of the scattered CO molecules in the $v = 0$ (left) and $v = 1$ states (right) measured at $T_s = 973$ K for three different E_i (0.16, 0.42, and 0.84 eV). For molecules scattered in both $v = 0$ and 1 states, the rotational distribution is non-thermal and is strongly influenced by the E_i. The spectra are peak normalized for the sake of comparison. (Lower panel) Examples of the fit to the REMPI spectra ($T_s = 973$ K, $E_i = 0.16$, 0.42, and 0.84 eV) in the Q(1,1) band region using a fit function as a sum of the individual Q(1,1) and O(0,0) components. The individual Q(1,1) and O(0,0) components are also shown.

distributions for $v = 1$ become broader with increasing T_s, whereas those for $v = 0$ do not change significantly. In order to correct for these effects in the evaluation of vibrational excitation probabilities, the angular distributions were fit to a peak normalized Gaussian function with the following form:

$$f(\theta) = \exp\left[-\frac{(\theta - \theta_0)^2}{2\sigma^2}\right].$$

The parameter σ (see Table II) is a measure of the width of the distribution and θ_0 represents the specular reflection angle.

At $E_i = 0.16$ and 0.84 eV, due to experimental limitations, the angular distributions for the molecules in $v = 1$ could not be measured accurately. In the absence of these values we make some approximations in order to account for the correction arising due to spatial dilution. At $E_i = 0.84$ eV

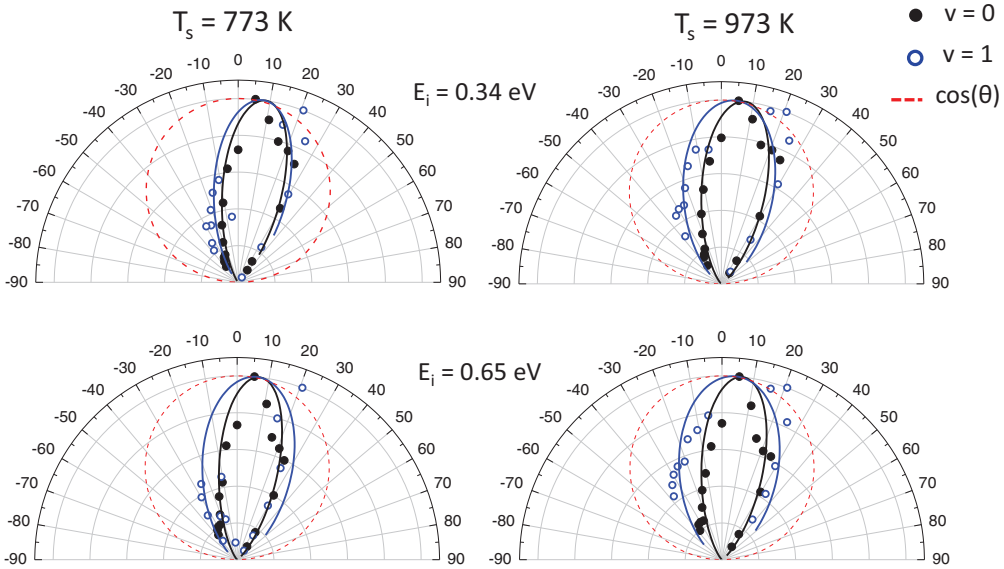

FIG. 4. Angular distributions observed for the scattered $v = 0$ (filled circles) and 1 (open circles) molecules measured at 773 and 973 K for two different E_i. For a given T_s the distributions for $v = 1$ are broader than those for the $v = 0$ and their width increases with T_s. The lines are the fits to the data using a Gaussian function as described in text. For the $v = 1$, due to significant background contribution the points between 0° and 10° are excluded. Note that the distributions observed are much narrower than the cosine distribution (red dashed curve) indicating that the direct inelastic scattering is the dominant channel.

TABLE II. The parameters obtained from the angular distribution measurements at different T_s and E_i values. The angular distributions were fit to a normalized Gaussian function. The parameter σ is a measure of the width of the distribution and θ_0 is the peak of the angular distribution. For $E_i = 0.16$ and 0.84 eV, the angular distributions for $v = 1$ could not be measured accurately due to experimental limitations. The uncertainties on σ and θ_0 are $\pm 1^\circ$ and $\pm 2^\circ$ for the $v = 0$ and 1, respectively.

		$v = 0$		$v = 1$	
E_i (eV)	T_s (K)	σ (deg)	θ_0 (deg)	σ (deg)	θ_0 (deg)
0.16	573	17	8	na	na
	773	17	5	na	na
	973	19	4	na	na
0.34	573	17	9	12	10
	773	16	9	19	8
	973	17	7	24	4
0.42	573	16	8	18	11
	773	16	7	20	8
	973	16	6	24	5
0.50	573	16	9	16	13
	773	16	8	22	6
	973	17	7	26	4
0.65	573	15	8	13	11
	773	16	7	24	6
	973	16	6	27	4
0.84	573	15	7	na	na
	773	15	6	na	na
	973	14	6	na	na

the correction factor for the angular distribution is assumed to be identical to that for $E_i = 0.65$ eV. This is reasonable because in this small range of E_i (0.65–0.84 eV), the scattering dynamics are expected to remain unchanged resulting in similar angular distributions. At $E_i = 0.16$ eV this correction factor is expected to be the biggest as trapping/desorption is the dominant channel for the vibrational excitation (this is discussed in more detail below). At this incidence energy, if all the $v = 1$ molecules arise via trapping/desorption and if the sticking probability were unity, the angular distribution is expected to follow a cosine distribution. In this case the correction factor due to the angular distribution is about 2 – we take this as an upper limit to the correction. The temporal profiles for the scattered molecules in $v = 0$ and 1 were measured individually at different T_s for each E_i and the correction for the temporal dilution was calculated in a similar manner.

Since the REMPI signal is proportional to number density, for a given flux, the detection sensitivity depends on the velocity at which the molecules move through the probe volume. However, due to insufficient signal-to-noise ratio, the speed distribution of the scattered molecules in $v = 1$ could not be measured using the time-of-flight methods that were employed in similar experiments with NO/Au(111).[7] Nonetheless, recently reported measurements on the NO/Au(111) system[21] show that in systems exhibiting EHP-V transfer, vibration is weakly coupled to translation. Based on this it is reasonable to assume that the velocity distributions for the scattered molecules in the $v = 0$ and 1 states are similar, resulting in only a small correction, which we neglect.

The absolute vibrational excitation probabilities obtained as a function of T_s measured at six different translational incidence energies are shown in Fig. 5. For a given translational incidence energy, the vibrational excitation probabilities increase with increasing T_s. Also shown (red dashed line) are the fits to the observed data with an Arrhenius

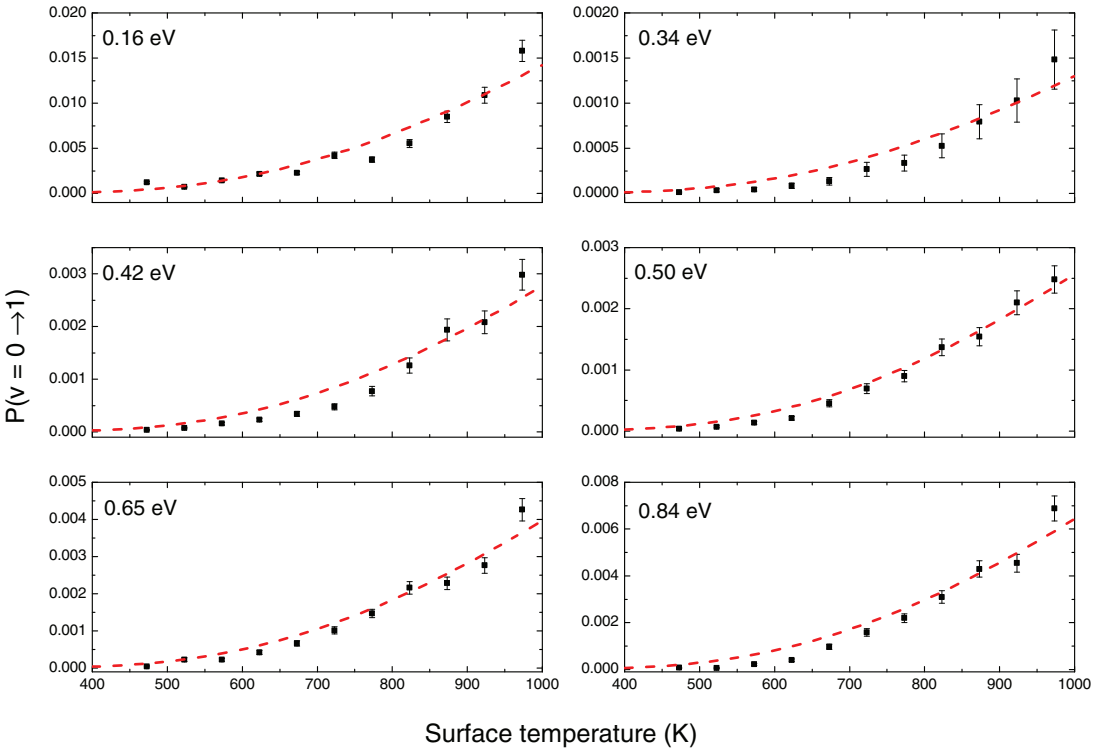

FIG. 5. Absolute vibrational excitation probabilities ($v = 0 \rightarrow 1$) as a function of surface temperature measured at different E_i. Note that the vertical scale is different in each of the plots. The dashed curve (red) represents the fit using the Arrhenius equation (see text).

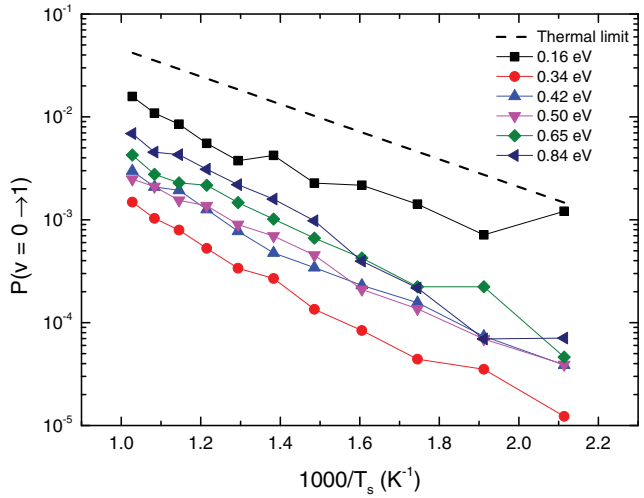

FIG. 6. Arrhenius plot for the observed vibrational excitation probabilities at different T_s measured at different incidence energies. The dashed curve depicts the fraction of $v = 1$ molecules as expected from thermal equilibrium (thermal limit). The error bars have been omitted in this plot for the sake of clarity.

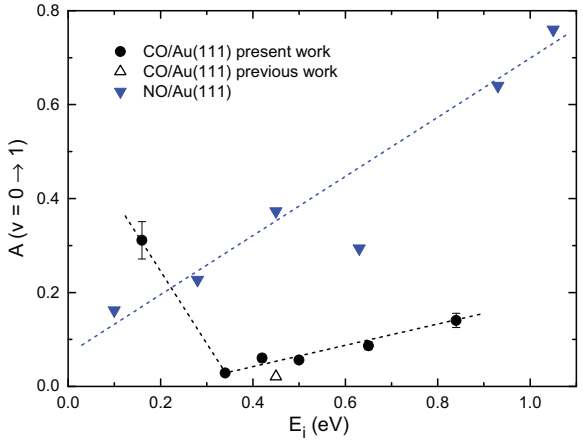

FIG. 8. Pre-factors obtained from the Arrhenius fit at different incidence energies (black dots) for CO. The downward pointing triangles (blue) are the pre-factors previously reported for NO vibrational excitation ($v = 0 \rightarrow 1$) upon scattering from Au(111).[7] The pre-factors for CO first decrease and then increase with E_i in contrast to those for NO, which increase monotonically with E_i. The upward pointing triangle denotes the previously reported value.[15] The dashed lines are shown purely as a guide to the eye to highlight the observed trends.

equation,

$$P(v = 0 \rightarrow 1) = A(E_i) \times \exp\left(-\frac{\Delta E_{vib}}{kT_s}\right),$$

where ΔE_{vib} is the CO $v = 0 \rightarrow 1$ vibrational energy gap (2143 cm^{-1}), k is the Boltzmann constant, T_s is the temperature in Kelvin, and $A(E_i)$ is the incidence translational energy dependent pre-factor, which may vary between 0 and 1. Note that $A(E_i) = 1$ corresponds to thermal equilibrium. Figure 6 shows the results of Fig. 5 as an Arrhenius plot. All vibrational excitation probabilities are one-tenth of the thermal limit – shown as a dashed line – or less, except at the lowest incidence energies and surface temperatures.

The E_i dependence of the vibrational excitation probabilities is shown in Fig. 7. These values are plotted for different values of T_s. Both above and below 0.34 eV, the vibrational excitation probabilities increase. This is an indication that the dynamics of scattering changes at low incidence energy. For the sake of comparison, the trapping probabilities (at 100 K) reported by Rettner are also shown in Fig. 7 (inset). This curve shows that the trapping probability is significantly large at low E_i – hence, we expect that at $E_i = 0.16$ eV the vibrational excitation has a significant contribution from trapping/desorption.

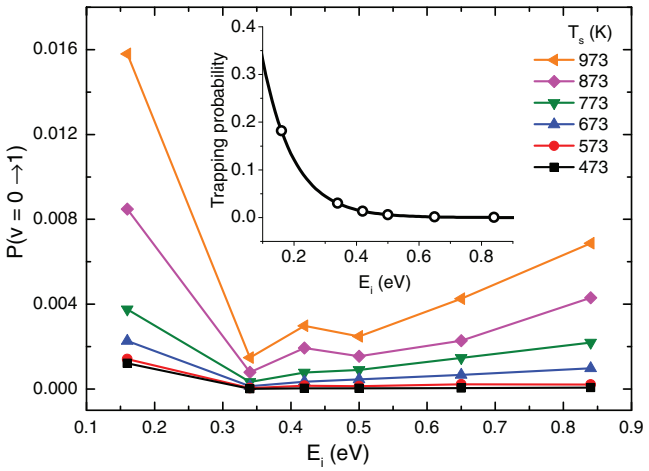

FIG. 7. The vibrational excitation probabilities as a function of the E_i for a given T_s. Clearly, the vibrational excitation probabilities first decrease and then increase with the E_i. The error bars have been omitted for the sake of clarity. Also shown in the inset is the trapping probability of CO on Au(111) at a surface temperature of 100 K reported by Rettner.[16] The open circles denote the E_i at which the present measurements were carried out.

The pre-factors obtained from the Arrhenius fits are plotted versus E_i in Fig. 8. Also shown here are the pre-factors reported for the NO/Au(111) system.[7] The pre-factors for CO/Au(111) are smaller by about a factor of 5 (except at $E_i = 0.16$ eV which is influenced by trapping/desorption) as compared to NO/Au(111) indicating that the magnitude of the non-adiabatic coupling strength in case of CO is only somewhat weaker than that for NO.

The vibrational excitation observed via the trapping desorption channel raises an important question: Do the "trapped" molecules completely thermalize their vibration before they desorb or not? In order to answer this question, one needs to compare the residence time of the CO molecules trapped on the surface with the timescale for the vibrations to come to equilibrium with the surface.

Temperature programmed desorption measurements show that the binding energy of CO on Au(111) is approximately 0.14 eV and the Arrhenius pre-factor is the order of 10^{13} Hz.[22] Based on these values, the estimated residence time (inverse of the desorption rate constant, obtained using Arrhenius equation for desorption) of CO molecules trapped on the Au(111) surface ranges from 10^{-11} to 10^{-13} s in the temperature range of 300–1000 K.

The vibrational relaxation rate of the adsorbed molecules is a measure of the timescale required for the vibrational degree of freedom of the trapped molecules to come to thermal equilibrium with the surface. Previous work shows that the vibrational relaxation timescales of CO adsorbed on

metal surfaces such as Pt and Cu are of the order of a few picoseconds.[1,23] If one assumes that the vibrational relaxation times are similar in the present case, then at higher temperatures (shorter residence times) there could be a situation that the molecules desorb before the vibrational degree of freedom is in equilibrium with the surface. Such an effect indeed has been reported for NO desorbing from Pt(111).[24] However, to the best of our knowledge the vibrational relaxation time for CO adsorbed on Au(111) is not known. More importantly, whether vibrational relaxation timescales are of the order of picoseconds for all metal molecule systems, irrespective of the strength of the interaction (physisorption vs. chemisorption) is an open question still. In absence of this information, it is difficult to say if in the present case the CO molecules have vibrationally equilibrated before desorption or not.

An additional remark we make here is regarding the mechanism of vibrational excitation in the trapping desorption channel. We believe that in this case too (similar to the direct scattering) the vibrational excitation occurs predominantly via the EHP-V mechanism simply because it is much more probable than energy transfer via phonons which involve multi-phonon transitions. A quantitative comparison of the rates of EHP-V vs. phonon-adsorbate energy transfer again requires the knowledge of the vibrational relaxation timescales which is presently unavailable. Some aspects of this question are currently being pursued in our lab by looking at the relaxation of vibrationally excited CO molecules on a clean Au(111) surface, and hopefully these measurements will be able to shed more light on this issue in the near future.

In summary, in this work we have carried out comprehensive measurements of the $v = 0 \rightarrow 1$ vibrational excitation probabilities for CO scattering from Au(111) as a function of the translational incidence energy and surface temperature. Our measurements show that the angular distributions of the scattered molecules are narrow and that for a given E_i, the vibrational excitation probabilities are strongly dependent on T_s. These observations are consistent with EHP-V energy transfer occurring via a single bounce, direct scattering event. The vibrational excitation probability at a fixed surface temperature was also found to increase with increasing E_i. However, at the lowest E_i (0.16 eV) the vibrational excitation probability and Arrhenius pre-factor (A) values were observed to be exceptionally high. We attribute this to the increased contribution of trapping/desorption at low E_i.

ACKNOWLEDGMENTS

A.M.W. would like to acknowledge the support from the Alexander von Humboldt Foundation.

APPENDIX: VIBRATIONAL EXCITATION PROBABILITIES AT DIFFERENT E_i AND T_s

See Table III for details.

TABLE III. The absolute vibrational excitation probabilities $P(v = 0 \rightarrow 1)$ and their uncertainties (ΔP) as a function of surface temperature measured at different translational incidence energies.

	$E_i = 0.16$ eV		$E_i = 0.34$ eV		$E_i = 0.42$ eV	
T_s (K)	$P(v = 0 \rightarrow 1)$	ΔP	$P(v = 0 \rightarrow 1)$	ΔP	$P(v = 0 \rightarrow 1)$	ΔP
473	1.2×10^{-3}	1×10^{-4}	1.2×10^{-5}	7×10^{-6}	3.9×10^{-5}	7×10^{-6}
523	7.1×10^{-4}	7×10^{-5}	3×10^{-5}	2×10^{-5}	7×10^{-5}	1×10^{-5}
573	1.4×10^{-3}	1×10^{-4}	4×10^{-5}	2×10^{-5}	1.6×10^{-4}	2×10^{-5}
623	2.2×10^{-3}	2×10^{-4}	8.4×10^{-5}	3×10^{-5}	2.3×10^{-4}	3×10^{-5}
673	2.3×10^{-3}	2×10^{-4}	1.3×10^{-4}	4×10^{-5}	3.4×10^{-4}	5×10^{-5}
723	4.2×10^{-3}	3×10^{-4}	2.7×10^{-4}	8×10^{-5}	4.8×10^{-4}	6×10^{-5}
773	3.8×10^{-3}	3×10^{-4}	3.4×10^{-4}	9×10^{-5}	7.7×10^{-4}	9×10^{-5}
823	5.5×10^{-3}	4×10^{-4}	5.3×10^{-4}	1×10^{-4}	1.3×10^{-3}	1×10^{-4}
873	8.5×10^{-3}	6×10^{-4}	7.9×10^{-4}	2×10^{-4}	1.9×10^{-3}	2×10^{-4}
923	1.1×10^{-2}	9×10^{-4}	1.0×10^{-3}	2×10^{-4}	2.1×10^{-3}	2×10^{-4}
973	1.6×10^{-2}	1×10^{-3}	1.5×10^{-3}	3×10^{-4}	3.0×10^{-3}	3×10^{-4}
	$E_i = 0.50$ eV		$E_i = 0.65$ eV		$E_i = 0.84$ eV	
T_s (K)	$P(v = 0 \rightarrow 1)$	ΔP	$P(v = 0 \rightarrow 1)$	ΔP	$P(v = 0 \rightarrow 1)$	ΔP
473	4×10^{-5}	1×10^{-5}	5×10^{-5}	1×10^{-5}	7×10^{-5}	2×10^{-5}
523	7×10^{-5}	1×10^{-5}	2.2×10^{-4}	5×10^{-5}	7×10^{-5}	2×10^{-5}
573	1.4×10^{-4}	2×10^{-5}	2.2×10^{-4}	4×10^{-5}	2.2×10^{-4}	4×10^{-5}
623	2.1×10^{-4}	3×10^{-5}	4.2×10^{-4}	6×10^{-5}	4.0×10^{-4}	6×10^{-5}
673	4.5×10^{-4}	6×10^{-5}	6.6×10^{-4}	7×10^{-5}	10×10^{-4}	1×10^{-4}
723	6.9×10^{-4}	8×10^{-5}	1.0×10^{-3}	9×10^{-5}	1.6×10^{-3}	2×10^{-4}
773	9.0×10^{-4}	9×10^{-5}	1.5×10^{-3}	1×10^{-4}	2.2×10^{-3}	2×10^{-4}
823	1.4×10^{-3}	1×10^{-4}	2.2×10^{-3}	2×10^{-4}	3.1×10^{-3}	3×10^{-4}
873	1.5×10^{-3}	1×10^{-4}	2.3×10^{-3}	2×10^{-4}	4.3×10^{-3}	4×10^{-4}
923	2.1×10^{-3}	2×10^{-4}	2.8×10^{-3}	2×10^{-4}	4.5×10^{-3}	4×10^{-4}
973	2.5×10^{-3}	2×10^{-4}	4.3×10^{-3}	3×10^{-4}	6.9×10^{-3}	5×10^{-4}

[1]H. Arnolds, Prog. Surf. Sci. **86**(1-2), 1 (2011).
[2]J. C. Tully, Annu. Rev. Phys. Chem. **51**, 153 (2000).
[3]A. M. Wodtke, D. Matsiev, and D. J. Auerbach, Prog. Surf. Sci. **83**(3), 167 (2008).
[4]B. D. Kay, T. D. Raymond, and M. E. Coltrin, Phys. Rev. Lett. **59**(24), 2792 (1987).
[5]C. T. Rettner, F. Fabre, J. Kimman, and D. J. Auerbach, Phys. Rev. Lett. **55**(18), 1904 (1985).
[6]R. Cooper, C. Bartels, A. Kandratsenka, I. Rahinov, N. Shenvi, K. Golibrzuch, Z. S. Li, D. J. Auerbach, J. C. Tully, and A. M. Wodtke, Angew. Chem. Int. Edit. **51**(20), 4954 (2012).
[7]R. Cooper, Z. S. Li, K. Golibrzuch, C. Bartels, I. Rahinov, D. J. Auerbach, and A. M. Wodtke, J. Chem. Phys. **137**(6), 064705 (2012).
[8]M. Born and R. Oppenheimer, Ann. Phys. **389**(20), 457 (1927).
[9]Y. H. Huang, C. T. Rettner, D. J. Auerbach, and A. M. Wodtke, Science **290**(5489), 111 (2000).
[10]J. D. White, J. Chen, D. Matsiev, D. J. Auerbach, and A. M. Wodtke, Nature (London) **433**(7025), 503 (2005).
[11]M. Head-Gordon and J. C. Tully, J. Chem. Phys. **103**(23), 10137 (1995).
[12]N. Shenvi, S. Roy, and J. C. Tully, Science **326**(5954), 829 (2009).
[13]N. Shenvi, S. Roy, and J. C. Tully, J. Chem. Phys. **130**(17), 174107 (2009).
[14]S. Monturet and P. Saalfrank, Phys. Rev. B **82**(7), 075404 (2010).
[15]T. Schäfer, N. Bartels, K. Golibrzuch, C. Bartels, H. Köckert, D. J. Auerbach, T. N. Kitsopoulos, and A. M. Wodtke, Phys. Chem. Chem. Phys. **15**(6), 1863 (2013).
[16]C. T. Rettner, J. Chem. Phys. **99**(7), 5481 (1993).
[17]Q. Ran, D. Matsiev, A. M. Wodtke, and D. J. Auerbach, Rev. Sci. Instrum. **78**(10), 104104 (2007).
[18]M. A. Hines and R. N. Zare, J. Chem. Phys. **98**(11), 9134 (1993).
[19]A. W. Kleyn and T. C. M. Horn, Phys. Rep. **199**(4), 191 (1991).
[20]See supplementary material at http://dx.doi.org/10.1063/1.4894814 for additional fits and best fit parameters.
[21]K. Golibrzuch, P. R. Shirhatti, J. Altschäffel, I. Rahinov, D. J. Auerbach, A. M. Wodtke, and C. Bartels, J. Phys. Chem. A **117**(36), 8750 (2013).
[22]D. P. Engelhart, personal communication (2014).
[23]H. Ueba, Prog. Surf. Sci. **55**(2), 115 (1997).
[24]M. Asscher, G. A. Somorjai, and Y. Zeiri, J. Chem. Phys. **81**(3), 1507 (1984).